Anisotropy of Radiation Damage in Electron-Bombarded Hexagonal Metals. I. Damage Production and Recovery for Monocrystalline Cobalt, Zinc, and Cadmium

F. Maury, P. Vajda, A. Lucasson, and P. Lucasson
Equipe de recherches du Centre National de la Recherche Scientifique, Laboratoire de Chimie Physique, F91405 Orsay, France
(Received 24 May 1973)

Monocrystalline specimens of cobalt, zinc, and cadmium of various crystallographic orientations were irradiated by electrons in the energy range 0.4–1.7 MeV at liquid-helium temperature and the respective electrical-resistivity-change rates and annealing spectra in the stage I were measured. In cobalt, the maximum defect production rate occurred for the specimen bombarded perpendicularly to the (0001) plane, the minimum rates were measured for the $(11\bar{2}0)$ samples. The apparent threshold energies for displacement vary between 450 and 500 keV, in the likely order: (0001), $(30\bar{3}4)$ and $(10\bar{1}0)$, $(30\bar{3}8)$, $(11\bar{2}0)$. The largest differences in the recovery behavior of cobalt were exhibited at low energies by the $(11\bar{2}0)$ and (0001) samples. For zinc, it is difficult to distinguish between different thresholds because of the big angular spread of the electron beam at the relatively low threshold energy of $\sim$ 350 keV. The production rates increase in the order (0001), $(11\bar{2}0)$, $(30\bar{3}4)$. Maximum recovery of the entire state I is observed for the (0001) sample, while the various substages behave quite differently as a function of crystal orientation. In cadmium, complex subthreshold behavior was observed and attributed to impurity effects. After separation of these phenomena, we deduce a minimum E_d of 630–650 keV for the (0001) orientation; after a size-effect correction, the measured resistivity-change rates are smallest for (0001), followed by $(30\bar{3}8)$ and $(11\bar{2}0)$. Two recovery regions are observed in the stage I: 4–6 and 6–9 °K; at low energies, the recovery of the $(30\bar{3}8)$ sample is smallest in the first region, and at high energies, it is maximal in both regions.

I. INTRODUCTION

The basic problem in radiation-damage studies remains the determination of the "true" threshold energy $T_d(\theta, \varphi)$ for producing a stable Frenkel pair when an atom is projected in a crystal direction (θ, φ). The complete solution of the problem results in the knowledge of the displacement probability function $p(T, \theta, \varphi)$, which depends on the kinetic energy T initially transmitted to the primary knock-on atom:

$$p(T, \theta, \varphi) = 0 \quad \text{if } T < T_d(\theta, \varphi)$$
$$= 1 \quad \text{if } T \geq T_d(\theta, \varphi) . \tag{1}$$

In polycrystalline specimens, one obtains the observed probability by integrating all these "step" functions over the space

$$P_d(T) = \int p(T, \theta, \varphi)\, d\Omega \Big/ \int d\Omega , \tag{2}$$

with $d\Omega = \sin\theta\, d\theta\, d\varphi$. The question has been treated theoretically in computer calculations by the Brookhaven group,[1,2] and it was shown—at least for cubic metals—that the threshold energy surface $T = T_d(\theta, \varphi)$ contained distinct minima corresponding to specific low-index crystallographic directions. (Jan and Seeger[3] used the results of Ref. 1 for fcc copper to give this surface an analytical form.) Thus, it was suggested[2] that the function $P_d(T)$ could be reasonably well approximated by a finite sum of step functions

$$P_d(T) = \sum_i p_i(T)\delta\Omega_i \Big/ \sum_i \delta\Omega_i , \tag{3}$$

where the $\delta\Omega_i$'s are the solid angles surrounding these particular directions. The number i and the quantitative parameters of the step functions would be obtained by comparison with experiment.

The direct correlation with this threshold energy surface of the interatomic potential $U(r)$, where r is the separation distance between two atoms, showed the importance of having additional data available to provide, eventually, parameters for $U(r)$ and to obtain computed results of adequate magnitude.

A series of experimental papers followed, which confirmed the predictions and stressed the role of correlated collisions, especially in the closest-packed directions of the lattice. For semiconductors, where as early as 1954 Kohn[4] had predicted an anisotropic threshold energy, this anisotropy has been observed in germanium[5] and silicon,[6,7] both of diamond structure. Anisotropy of resistivity changes under electron irradiation was reported for hexagonal graphite.[8] The first damage-rate measurements on metals were done with cubic crystals: fcc copper,[9–11] and gold,[11,12] and bcc iron[13] and tantalum.[14] Also, recent results obtained in this laboratory on molybdenum[15] showed a marked difference between the three principal crystal directions. The construction of high-voltage electron microscopes enabled the direct observation of damage anisotropy, and corresponding studies were undertaken on copper,[16] nickel,[17] and cobalt.[18]

Differences in recovery behavior have been noted on copper and iron whiskers,[19] and detailed studies were made with the $I_{A,B,C}$ substages in copper[10,20] and with the I_B substage of aluminium.[21] Very pronounced effects have also been seen in

molybdenum.[15] In their thorough investigation of thermal-neutron damage in hcp cadmium, Coltman *et al.*[22] observed recovery anisotropy in isotropically bombarded monocrystalline specimens when the angle between the direction of the measuring current and the c axis was varied.

The first systematic studies of the effect of electron bombardment on the resistivity change of differently oriented crystals of hexagonal metals were undertaken in this laboratory together with C. Minier of the C.E.N., Grenoble, and preliminary results were reported for monocrystalline cobalt.[23,24] These studies had been prompted by the experiments performed on polycrystalline specimens of several hcp metals—magnesium,[25,26] cadmium,[27] zinc,[28] zirconium,[29] titanium[30]—which all proved that it was impossible to fit experimental damage-rate results with a single-step displacement probability function. Two and sometimes three step functions (or linear functions with two thresholds, which is equivalent) were needed to match a theoretical function to the data, and it seemed reasonable to us to attribute this to the greater anisotropy of the hcp metals as compared to the cubic ones. Moreover, no computer calculations comparable to those for the fcc metals[1] and for the bcc metals[2] were existing to provide a theoretical framework. For this reason, and to unravel the field, we have undertaken a systematic study of three hexagonal metals: the monocrystalline cobalt, zinc, and cadmium—chosen such that the c/a ratio of their unit cell was either close to the ideal value $(\frac{8}{3})^{1/2}$ (cobalt: 1.63) or had an extreme value (zinc: 1.86 and cadmium: 1.89).

In Sec. II, we shall describe the specimen preparation—an essential part of the program—and the experimental facilities; in Sec. III, the obtained resistivity-change rates and the subsequent recovery behavior are presented in detail. The physical relevance of the results and the necessary corrections imposed by the experimental conditions are discussed in Sec. IV.

In the following paper, hereafter referred to as Paper II, we shall put forward a model for damage creation in hexagonal metals and, by using various sets of threshold energies as parameters, try to match computed defect production curves to the obtained experimental damage-rate data. With the thus-established optimal set of T_d's, we shall possess the means to determine, to a certain extent, appropriate potential parameters.

II. EXPERIMENTAL

A. Specimen Preparation

1. Cobalt

Platelets 0.3–0.5 mm thick were spark cut in various selected directions from a pulled single crystal obtained from C. Minier of Grenoble. These platelets were then mechanically polished down to about 100 μ with emery paper up to grade 800, finishing with a diamond paste to give a mirrorlike surface on both sides. Rectangular strips of 15-mm×1.2-mm size were then cut out using a fine watchmaker file so that excessive mechanical damage would not be introduced during this procedure. (To facilitate the polishing and cutting process, the specimen had been glued to a Plexiglass disk). The final thinning to ~20 μ was performed by applying an electrochemical-polishing method, with 50% HCl plus 50% C_2H_5OH as an electrolyte.[31] A special specimen holder was designed so as to prevent excessive attack at the edges; 0.2-mm tantalum wire spot welded to the sample served as contact material. The thinning rate in this system is rather rapid; ~100 μ/min; the resultant foils were ~0.5 mm large and had a brilliant appearance. In order to remove remaining stresses and to reduce their impurity contents, the samples were annealed for several hours at 700 °C in a hydrogen atmosphere. Subsequent x-ray analysis was performed on the specimens: A few of them, which showed twin structure, were discarded. The thus-prepared samples were parallel to the following crystal planes: (0001), $(10\bar{1}0)$, $(11\bar{2}0)$, $(30\bar{3}4)$, and $(30\bar{3}8)$. Their resistivity ratio was $\mathcal{R} = \rho_{300}/\rho_{4.2\,°K} = 10$–$20$.

2. Zinc

The same polishing and cutting procedure as for cobalt was used for the ~1-mm-thick zinc platelets spark cut from a $5N+$ crystal obtained from Materials Research Corporation (MRC). Special care had to be taken to prevent them from cleaving in the (0001) plane, which is an easy slip plane in zinc. Thus, many specimens of the intermediate orientations between the basal and the prismatic planes broke during the preparation or—when they had survived that—later, during the cooling in the cryostat, due to thermal stresses. (No such problems occurred for cadmium, though it obeys the same slip conditions and has an equally abnormal c/a ratio.) The final thinning was done by chemical polishing, using a solution of 20 g of CrO_3 and 1.5 g of Na_2SO_4 in 5 ml of HNO_3 + 95 ml of H_2O.[31] This is an excellent polishing solution, which very uniformly removes ~7 μ/min (each side) and leaves a brilliant surface of high crystallographic quality, as shown by x-ray analysis. The final specimens were longer than those of cobalt: They measured 20×0.5 mm and were 25–30 μ thick. They were annealed in vacuum (< 10^{-7} Torr) at 300 °C for 30 h and had an $\mathcal{R} = 1500$–3000, not corrected for surface scattering. Specimens of orientations parallel to the (0001), $(11\bar{2}0)$, and $(30\bar{3}4)$ planes were obtained. We want to remark in this context that

the $(11\bar{2}0)$ crystals had always exhibited the lowest values of $\mathcal{R}$ (the same was observed for cadmium), which can be understood as preferential migration (and subsequent pinning) of impurities into the crystal along the dislocation lines.

3. Cadmium

The cadmium platelets spark cut from a $5N+$ MRC crystal were treated in the same way as zinc, with the advantage that they were much less fragile. On the other hand, their great softness had to be considered during handling to prevent bending. The chemical polish was performed with a solution of 15-g-CrO_3 in 0.2 ml of H_2SO_4 + 100-ml H_2O.[31] The thinning rate at room temperature is roughly 4 μ/min. The resultant foils of 20×0.5-mm size were ~30 μ thick and were afterwards annealed at 150 °C for 30 h at $< 10^{-7}$ Torr. Their noncorrected resistivity ratio was then $\mathcal{R}=2000-3500$ (see also the remark made for zinc).

The relevant characteristics of the used specimens are collected in Table I. Thickness determinations were first made by calculating the geometrical shape factor from the electrical resistance measurements; then, after the experiments, the thickness was measured directly by means of a micrometer (with a resolution of 1 μ). The results coincided to within 10%.

B. Irradiation Facility

The specimens were irradiated by 0.40–1.70-MeV electrons coming from the Cockroft-Walton accelerator of the Laboratoire de Chimie Physique at Orsay.[32] For this purpose, they were soft soldered to an insulated sample holder, which itself was placed in the sample chamber of a liquid-helium cryostat[33] attached to the beam tube of the accelerator. The specimens were exposed to a controllable jet of liquid helium, so that even during irradiation their temperature could be kept close to 4.2 °K. The sample holder provides the possibility of soldering 10–12 strips to be bombarded at the same time by the same flux of particles, thus permitting the simultaneous irradiation of various crystalline orientations, which is obviously an important factor for the comparison of the induced effects. Before reaching the specimens, the electron beam passes through a 5.6-μ-thick window of Havar (a nickel-cobalt alloy) and through 2-mm helium gas at the irradiation temperature, so that it is already spread out to a certain degree when entering the crystal. This and the subsequent scattering in the specimen itself have to be taken into account and will be discussed in Sec. IV.

For the electrical measurements—all made at 4.2 °K—reference samples were soldered to the nonbombarded half of the sample holder, and precisely regulated currents (generally several-hundred mA regulated to $\pm 10^{-5}$) were sent through the specimen and the reference wired in parallel. The difference in voltage drops through both and thus the corresponding resistance changes were measured directly.[34] The precision for the determination of the resistivity changes was 10^{-11} Ω cm for cobalt, 5×10^{-13} Ω cm for zinc, and 1.5×10^{-13} Ω cm for cadmium. The reference samples were usually prepared of the same material as the examined crystal to ensure identical temperature behavior; in some cases, however, especially for zinc, where its extreme fragility at low temperature advised us not to double the risk of breaking both sample and reference or either, polycrystalline foils of about the same resistivity ratio were employed. Special precautions were taken during the mounting of the foils, soldering them relatively loosely to the sample holder and using holder material of about the same thermal expansion properties, in order not to exert too much mechanical stress during contraction of the system while cooling down. Even then, the survival ratio for zinc was not higher than 1 : 3.

The recovery measurements were performed *in situ*. The temperature control was assured by miniature platinum resistance thermometers in the range 6–300 °K and by Allen-Bradley 47-Ω and/or 220-Ω, $\frac{1}{8}$-W carbon resistors between 4 and 20 °K. An AuFe (0.07-at.%-Fe) - chromel thermocouple was used as an auxiliary thermometer over the whole temperature range.

TABLE I. Specimen characteristics.

Crystal	∥ to	Thickness (μ)	$\mathcal{R}_{meas}$	$\mathcal{R}_{corr}$[a]
zinc	(0001)	25	3000	28.000
	$(11\bar{2}0)$	25	1500	3.800
	$(30\bar{3}4)$	30	3100	20.000
cadmium	(0001)	29	3600	40.000
	$(11\bar{2}0)$	30	2100	6.800
	$(30\bar{3}8)$	32	3300	22.000

[a]Correction due to size effect using the tables of F. Dworschak, W. Sassin, J. Wick, and J. Wurm, obtained from KFA Jülich/Aachen, Germany, Report No. Jül. -575-FN (1969) (unpublished).

III. RESULTS

A. Cobalt

1. Defect Production

Two independent irradiations were performed using different sets of specimens of various orientations which each time had been placed in different positions on the sample holder to avoid systematic errors due to an eventual beam inhomogeneity, which, despite all the precautions, like beam spreading by a 2-μ-thick aluminium foil at the en-

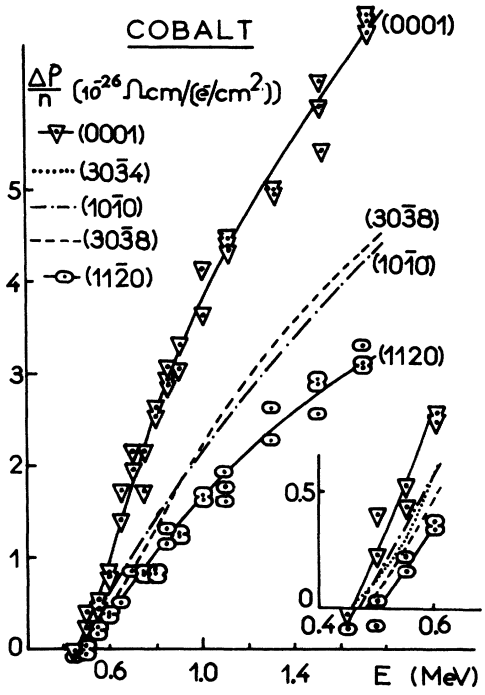

FIG. 1. Resistivity-change rates of cobalt crystals parallel to the (0001), (30$\bar{3}$8), (30$\bar{3}$4), (10$\bar{1}$0), and (11$\bar{2}$0) planes as a function of the incident electron energy. The drawn curves are eye-fits through the experimental points. The curves for the (30$\bar{3}$4) and the (10$\bar{1}$0) samples are practically coinciding and are shown as distinct only in the insert representing an enlarged view of the near-threshold area.

trance of the beam tube and beam sweaping, could still be produced by, e.g., edge scattering in the final diaphragm. Thus, not the absolute figures of the defect production rates were compared, but rather the relative values of the different orientations with regard to each other.

Figure 1 shows the resistivity-change rates per incident electron as a function of electron energy for various orientations of the cobalt crystals. We see at once that the (0001) specimen (basal plane perpendicular to the bombarding electron beam) yields by far the largest damage rates. The minimum damage rate is exhibited by the (11$\bar{2}$0) specimen, while the three other crystals possess intermediate values.

Another characteristic feature is the "visual" threshold energy, obtained by extrapolation of the eye-fitted curves to zero production rate. We have plotted the interesting part near the low-energy end in the insert of Fig. 1. The apparent threshold, not corrected for energy loss through the foils and for straggling, is smallest for the (0001) and highest for the (11$\bar{2}$0) crystals; the two extremes are ~450 and ~500 keV. The (30$\bar{3}$4) threshold seems to be as low as that for (0001) (450–460 keV), about the same can be said of the (10$\bar{1}$0) specimen (460 keV), while the (30$\bar{3}$8) specimen (~480 keV) is closer to the (11$\bar{2}$0) value; the agreement for the two runs was rather good.

Finally, we should like to remark that after thorough examination of the experimental points and of their scatter and especially after extending the measured values to 1.7 MeV, we do no longer attribute any significance to the structure in the production-rate curves as reported in our preliminary communication.[23]

2. *Recovery*

The recovery spectra in the recovery stage *I* of all the irradiated crystals have been investigated for various bombarding energies and it was found that the specimens which displayed extremal behavior in their damage-rate curves, (11$\bar{2}$0) and (0001), exhibited also the largest differences during recovery. In Fig. 2, we show the differentiated recovery spectra for all the orientations, presenting them in order of growing angle between the incident-electron direction and the *c* axis of the crystal. On the left-hand side are exposed the results of a low-energy (0.7-MeV) irradiation, on the right-hand side those of a high-energy irradiation (1.7 MeV). To have a coherent picture, we regard only the behavior during stage I, which is supposed to be finished at 60 °K; thus, the curves represent the resistivity recovery per degree in percent of the corresponding total recovery at 60 °K.

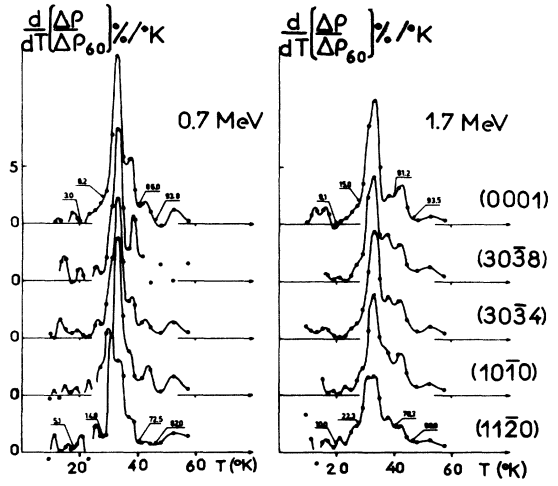

FIG. 2. Differentiated annealing spectra of five cobalt crystals of various orientations after a bombardment with 0.7 MeV (left-hand side) and with 1.7 MeV (right-hand side) electrons. The data are normalized to the respective recoveries at 60 °K. The numbers with arrows indicate the normalized annealed percentage at the corresponding temperature.

The general features correspond quite well to the spectra obtained by Sulpice *et al.*[35] for polycrystalline cobalt. However, the most important recovery peak, centered at 33 °K (I_C in their denomination), is itself decomposable into two subpeaks, which behave in an interesting way when going from one orientation to another: at 0.7 MeV, e.g., we observe the appearance of a shoulder for the $(30\bar{3}8)$ and $(30\bar{3}4)$ samples, which develops to a distinct peak at ~31 °K for $(10\bar{1}0)$ and becomes preponderant in the case of the $(11\bar{2}0)$ crystal. A regular evolution is also shown by the peak at 26 °K, which has its maximum amplitude for the $(11\bar{2}0)$ orientation and the minimum value for the (0001) orientation. The peak at 38 °K is most important in the case of the (0001) and $(30\bar{3}8)$ samples and smallest for the $(11\bar{2}0)$ crystal. At higher energies (right-hand side of Fig. 2), the differences between the orientations are reduced (the peak I_C itself is strongly diminished), the recovery stage around 43 °K has, in general, increased, while that which is between 50 and 60 °K has decreased.

There is an interesting point to be made here concerning the I_C peak. If one takes the whole peak without decomposing it (as in the case of Ref. 35), one obtains a half-width at half-maximum (HWHM) of $\Delta T \approx 2.5$ °K. This, at 33 °K and assuming a first-order reaction, corresponds to an activation energy of 0.04 eV. In their study of polycrystalline cobalt, however, Sulpice *et al.*[35] determined the activation energy of this substage to $E_A = 0.06$–0.07 eV. This discrepancy disappears if one considers that the peak is decomposed into two subpeaks with HWHM's of less than 1.5 °K. The distinctive behavior of the two subpeaks with regard to irradiated orientation in the case of the single crystals is a nice demonstration of the fine structure of the I_C peak and also of the possibilities opened by the study of monocrystals.

B. Zinc

1. Defect Production

As already mentioned in Sec. II, the zinc specimens were extremely fragile, so that we have got reproducible results only on three orientations, (0001), $(11\bar{2}0)$, and $(30\bar{3}4)$. Their resistivity-change rates as a function of the incident electron energy are plotted in Fig. 3; for comparison, we have included the damage-rate curve of a polycrystalline specimen, which had been irradiated simultaneously with the monocrystals. The picture differs markedly from the case of cobalt: Here, the highest damage rate is achieved by the $(30\bar{3}4)$ crystal and the lowest by the (0001) specimen. The curve corresponding to the $(11\bar{2}0)$ orientation is intermediate and follows closely that of the polycrystalline sample.

It is rather difficult to make any definite statement which concerns the threshold for defect creation, since the lowest electron energy readily obtainable in our experimental conditions was 400 keV. A tentative extrapolation taking into account the curvature of the production curves around 0.4 MeV leads to roughly the same value for all the three thresholds, ~350 keV. This does not necessarily mean that the threshold energy surface is isotropic, but is most probably due to the fact that at such low energies the electron beam is already spread out by the windows of the specimen chamber and the specimen itself to such an extent that it attains the "easiest" displacement direction in any case—independently of the initial incidence angle. The anisotropy in this case is only manifested in the defect production yield. We shall come back later to this problem of beam spread.

We should like to make one remark considering a correction which, in principle, has to be taken into account: This is the thickness correction, which for thin specimens of high resistivity ratio $\mathfrak{R}$, such as our zinc and cadmium crystals, could become important. In fact, the introduction of defects by irradiation adds to the residual resistivity of the specimen and thus diminishes its $\mathfrak{R}$ (annealing of damage has the inverse effect). We have examined the possible implications of this effect and found that, indeed, this correction was not negligible. The problem is complicated by the fact that, the thickness being not absolutely uniform, even variations of 2–3 μ out of 25–30 μ render a correction difficult and hazardous. Therefore, we have tried[34] to apply it empirically by plotting the resistivity change rates of each specimen at different energies as a function of sample resistivity at the beginning of each corresponding irradiation run. The observed progressive saturation effect permits the deduction of an effective thickness correction, which, in the case of zinc, turns out to be roughly the same for all the orientations, leaving the relative positions of the different curves practically unchanged. We shall see that this is not the case for cadmium.

2. Recovery

The recovery of electron-bombarded zinc occurs for its major part during stage *I*; thus, it had been found previously[28] that in polycrystalline specimens, irradiated at 4.4 °K, 98% of the introduced damage annealed out at 16 °K for a 0.6-MeV irradiation and 80% for a 1.7-MeV bombardment. Moreover, five recovery substages had been observed: I_A at 5 °K, I_B at 7 °K, I_C at 9.5 °K, I_D at 12.5 °K, and I_E at 15 °K, the most important ones being I_C and I_D.

We have made several 10-min anneals at selected temperatures so as to separate the different substages, for various bombarding energies. In Table

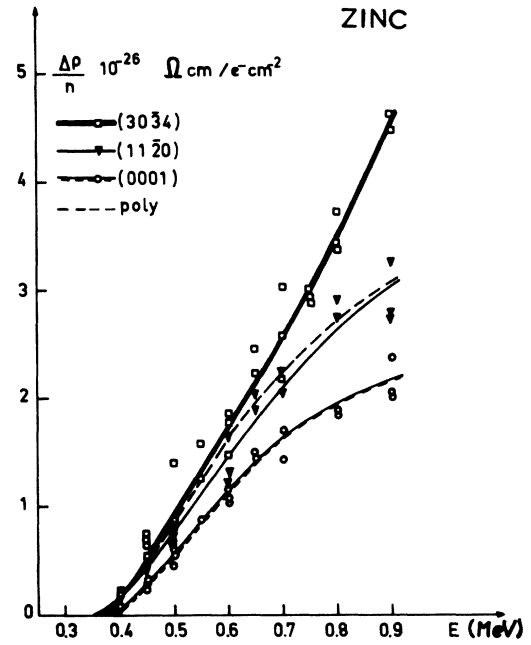

FIG. 3. Resistivity-change rates of zinc crystals parallel to the (0001), (11$\bar{2}$0), and (30$\bar{3}$4) planes as a function of incident electron energy. The drawn curves are eye-fits through the experimental points; the dashed curve is the damage rate of a polycrystal.

II, the results for the three employed orientations are presented together with those of a polycrystalline zinc specimen irradiated at the same time, for comparison. We note maximum recovery at all three energies for the (0001) sample, though the difference between the orientations tends to smear out with increasing electron energy. Looking more into details, we see that it is substage I_C of the (0001) specimen which greatly exceeds that of the others [46% at 0.5 MeV compared to 28–29% for the cases of (11$\bar{2}$0) and (30$\bar{3}$4)], while the tendency is reversed for substage I_D [61% for the (30$\bar{3}$4) sample and only 50% for the (0001) crystal]. The (11$\bar{2}$0) and the (30$\bar{3}$4) crystals are hardly distinguishable; there seems to be a slight difference for the substages I_A and I_B; the polycrystal is intermediate. The relative increasing importance of substage I_A for 0.9 MeV is in conformity with the earlier observations on polycrystals. Substage I_E seems to be growing with increasing electron energy; it was not monitored for the (30$\bar{3}$4) sample.

C. Cadmium

We have irradiated specimens of the orientations (0001), (11$\bar{2}$0), and (30$\bar{3}$8).

1. Subthreshold Effects

In a recent study of polycrystalline high-purity cadmium irradiated by energetic electrons,[27] we had observed that the resistivity-change rate per incident electron saturated with increasing electron fluence, first rapidly falling until 1×10^{15}–2×10^{15} electrons/cm^2, then decreasing slowly at higher fluences. The curves were parallel for all the energies investigated (0.5–1.7 MeV) and there was practically no difference between them for energies below 0.6 MeV. This phenomenon could neither be explained by electrical size effects nor by deviations from Matthiessen's rule and was attributed to a saturable subthreshold effect, due to very low concentrations of hydrogen atoms (introduced during the chemical thinning procedure)

TABLE II. Resistivity recovery of zinc during stage *I*.

			(0001)		(11$\bar{2}$0)		(30$\bar{3}$4)		poly	
E/MeV	T/°K	Sub-stage	$\Delta\rho_0$ nΩ cm	%	$\Delta\rho_0$ nΩ cm	%	$\Delta\rho_0$ nΩ cm	%	$\Delta\rho_0$ nΩ cm	%
0.5	6	I_A		1		0		1		1
	8	I_B		1.5		0.5		1.5		1.5
	11	I_C	0.18	47.5	0.24	29.5	0.40	29	0.30	38
	14	I_D		97.5		87		90		93
	20	I_E		100		92		...		...
0.6	6	I_A		0		1		0		0
	8	I_B		0		1		0		1
	11	I_C	0.31	40.5	0.34	30	0.55	29	0.38	37
	14	I_D		94		85		86.5		90
	20	I_E		98		93		...		94
0.9	6	I_A		10.5		11		10.5		11
	8	I_B		12		12		10.5		13
	11	I_C	0.48	47.5	0.43	40.5	1.04	42	0.63	46.5
	14	I_D		92.5		85		85		89
	20	I_E		98		92.5		...		95

loosely bound to some sites in which they had low resistivities and from which they were displaced into higher resistivity sites under electron bombardment. This subthreshold effect and the normal cadmium-atom displacement process were clearly separable in the annealing experiments: Most of the cadmium-recovery proper was accomplished below 6–10 °K, while the added "subthreshold" resistivity disappeared only after ~150 °K.

We have repeatedly observed analogous phenomena with our monocrystalline specimens, their behavior being dependent on preparation (purity, annealing treatment), and irradiation conditions (temperature, electron fluence). Strong anisotropy effects were noted both with the resistivity change rates and with the recovery curves for the three irradiated orientations (0001), (11$\bar{2}$0), and (30$\bar{3}$8). A remarkable correlation was also found between resistivity ratio $\mathcal{R}$ (i.e., purity), orientation, and anisotropy manifestation of the specimens. We have tentatively assigned the effects to hydrogen atoms trapped on different sites and in different quantities as concerns the specimen orientations, and which contribute to defect production and recovery according to different mechanisms, dependent on their crystallographic situation. The behavior remains very complex and is the subject of a different study (cf. Ref. 34).

In the present work, we have rather wanted to understand what is going on with the atoms of the crystal lattice itself: for this purpose, we have tried to separate the subthreshold effects using

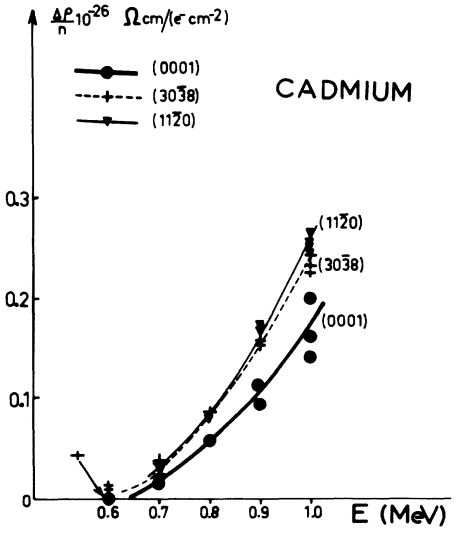

FIG. 4. Measured resistivity change rates of cadmium crystals parallel to the (0001), (11$\bar{2}$0), and (30$\bar{3}$8) planes as a function of the incident electron energy. The drawn curves are eye-fits through the experimental points.

their saturation properties by preirradiating the specimens with electrons of subthreshold energies (0.5 MeV). The results thus obtained give a more-or-less coherent picture of the cadmium-atom displacement processes and are presented in Sec. III C 2.

2. *Defect Production*

In Fig. 4, we present the measured resistivity change rates of the three irradiated orientations in the energy range up to 1 MeV. These raw data show minimum damage rates for the (0001) crystal, while those of the (11$\bar{2}$0) and (30$\bar{3}$8) specimens are essentially the same. As for the threshold energies, we deduce an E_d of slightly above 600 keV for the (0001) sample and slightly below for the (30$\bar{3}$8) crystal; an extrapolation of the (11$\bar{2}$0) data seems difficult because of the lack of experimental points at 0.6 MeV, but one is tempted to assign to this orientation an intermediate threshold of ~600 keV. For comparison, the threshold energy of polycrystalline cadmium had been previously[27] determined to 610 keV. In any case, as we shall see in Paper II, the observed apparent thresholds are much less significant for the manifestation of anisotropic defect production than differences in the production rates as a function of energy. As for the latter, we have to apply here the correction for the thickness effect, which we have discussed in Sec. III B 1. In fact, the (0001) specimen having the largest resistivity ratio (cf. Table I) requires also the biggest correction, while the least-pure specimen, (11$\bar{2}$0), needs the smallest one-the relative differences in production rates are increased; the corrected curves are plotted in Fig. 5.

3. *Recovery*

With the great majority of the introduced lattice defects annealing below 6 °K, in addition to the very low resistivity-change rates, which imposed correspondingly long irradiation times with small electron currents to avoid heating by the beam, plus the uncertainty of having really disposed of all the subthreshold effects by saturating them, we had problems obtaining reproducible recovery data. For the sake of getting an idea of the observed anisotropy, we present in Table III the annealing percentages in the two recovery regions for three different energies. One remarks two main features: (i) At lower energies, there is very little or no recovery above 6 °K, while at 1.7 MeV the situation is reversed—the recovery stage at 6–9 °K is larger than that at 4–6 °K. (ii) At lower energies, the (30$\bar{3}$8) specimen exhibits a smaller recovery stage at 4–6 °K and a larger one at 6–9 °K than the other orientations; at high energy, both recovery stages are more pronounced for this crystal.

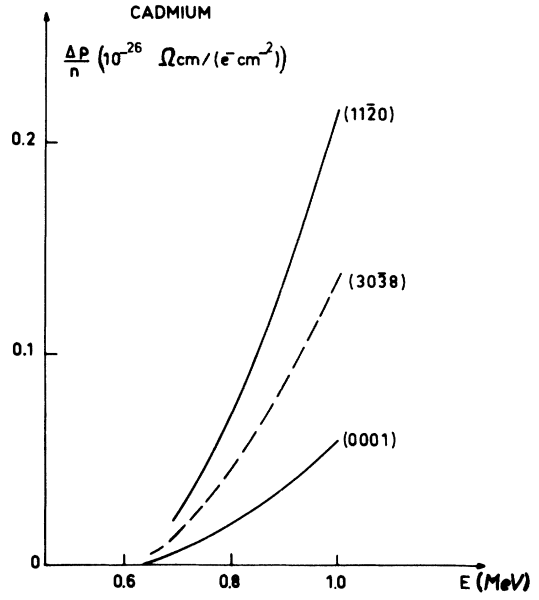

FIG. 5. Resistivity-change rates of cadmium crystals as a function of incident electron energy, after application of a size-effect correction to the results presented in Fig. 4.

IV. DISCUSSION

When relating the resistivity changes $\Delta\rho$ induced during the electron bombardment to the point defect formation, one has to introduce a characteristic quantity ρ_F, the resistivity of a Frenkel pair per unit concentration of atoms, such that

$$\Delta\rho/n = \sigma(E)\rho_F. \tag{4}$$

Here, n is the incident electron fluence and $\sigma(E)$ is the energy-dependent cross section for defect formation. This cross section is connected with the probability function $P_d(T)$ discussed in Sec. I:

$$\sigma(E) = \int_{T_d}^{T_{\max}} \frac{d\sigma}{dT} P_d(T)\, dT\,, \tag{5}$$

where $d\sigma/dT$ is the Rutherford differential scattering cross section.

In the case of a polycrystalline specimen, the interpretation of the results is reduced to the problem of comparing the experimentally obtained dependence $\Delta\rho(E)/n$ with a family of calculated cross sections of the type in Eq. (5) and, assuming a certain fixed value for ρ_F, derive the interesting function $P_d(T)$. One can fit the experimental results with a simple or a multiple-step function, each step corresponding to a particular displacement mechanism in the crystal lattice. From a certain transmitted energy on, roughly $T \gtrsim 2T_{d\,\min}$, one has to consider multiplication processes, i.e., the creation of more than one Frenkel pair per collision event (cascade formation). In our experiments, however, this correction is always small, its maximum being at 1.7 MeV and for the masses of the elements studied not greater than 10–20%.

In single-crystal specimens, where because of the distinct and not superposed single-step processes one would expect simpler damage mechanisms, the phenomenon is complicated by the finite thickness of the specimens. Suppose, we bombard a single crystal in a direction Δ_1, which is an easy displacement direction, with electrons of an energy E slightly above threshold. Since the maximum transmitted energy, $T_{\max} = T\cos^2\theta$ is only a little larger than T_{d1} in this direction, the recoil angle θ permitted for displacements remains small. And, as Erginsoy *et al.*[2] have shown, the threshold energy in a small solid angle Ω_1 around the direction Δ_1 being approximately constant the cross section becomes

$$\sigma(E) = \int_{T_{d1}}^{T_{\max}} \frac{d\sigma}{dT}\, dT\,. \tag{6}$$

This is no longer true when the electron energy is increased. In fact, the atoms recoiling in a direction Δ_i spanning an angle θ_i with the easy direction Δ_1 sufficiently large to reach other easy displacement regions will, from a certain moment on, possess enough energy to displace atoms in these regions. Moreover, this effect is enhanced by the fact that the differential cross section is proportional to $(\cos^3\theta)^{-1}$, thus favoring the displacements in directions which are inclined with respect to the incident electron direction. In the case of an irradiation in a direction Δ_2 which corresponds to a higher threshold than that of Δ_1 ($T_{d2} > T_{d1}$), it may happen that electrons which are not energetic enough to displace an atom into Δ_2 possess, nevertheless, a sufficient energy to transmit an atom an energy $T > T_{d1}$ into Δ_1. For example, in the case of bcc iron, where we possess numerical values for the threshold energy surface,[2] the principal directions have the following thresholds: $T_d^{(111)} = 38$ eV, $T_d^{(110)} = 34$ eV, $T_d^{(100)} = 17$ eV. In Fig. 6, we demonstrate an irradiation in the relatively difficult direction ⟨110⟩. This is a polar plot of the function $(\cos^3\theta)^{-1}$, which is proportional to $d\sigma/d\Omega$. The two

TABLE III. Resistivity recovery of cadmium.

E/MeV	T/°K	$\Delta\rho/\Delta\rho_0$ (%) (0001)	(30$\bar{3}$8)	(11$\bar{2}$0)
0.7	4–6	100	55–65	90
	6–9	1	10	0
0.9	4–6	80–100	70–85	80–100
	6–9	5–10	5–10	7–10
1.7	4–6	30	40	27
	6–9	35	47	43

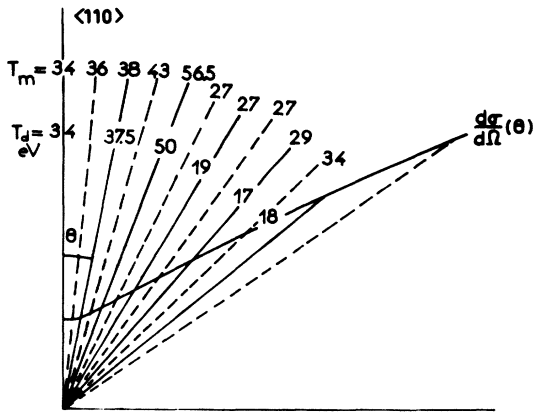

FIG. 6. Polar plot of the differential scattering cross section for a given energy around a ⟨110⟩ direction of bcc iron (using the results of Ref. 2). The two sets of numbers correspond, respectively, to the thresholds $T_d(\theta)$ in a certain direction θ off the ⟨110⟩ axis and to the maximum energy transmittable to an atom in the ⟨110⟩ direction corresponding to the threshold energy in the direction θ, $T_{max} = T_d(\theta)/\cos^2\theta$.

sets of numbers designate the energy thresholds in the direction in question, $T_d(\theta)$, and the maximum energy that an electron can transmit to an atom in the direction ⟨110⟩ when it possesses just the energy necessary to displace this atom in the direction θ: $T_{max} = T_d(\theta)/\cos^2\theta$. We see at once that before being able to displace an atom directly in the ⟨110⟩ direction ($T_d^{\langle 110\rangle} = 34$ eV), an electron with an energy corresponding to a $T_{max} = 27$ eV will produce a displacement in a direction with a $\theta \geq 30°$, which belongs to the easy displacement region around ⟨100⟩. Thus, we shall observe an apparent threshold energy of $T_d^{\langle 110\rangle} = 27$ eV, which is not at all a true image of the actual physical process. Moreover, due to the strong increase of $d\sigma/d\Omega$ with increasing θ, the production rate under these irradiation conditions will be greater than when bombarding directly in the direction ⟨100⟩.

For hexagonal metals, there are no model calculations like those existing for fcc[1] and bcc[2] crystals, but one can safely deduce that the situation will be analogous or slightly more complicated owing to the lesser symmetry of the hcp lattice. We shall prove this by presenting a model in Paper II.

Until now, we have supposed that the electron energy had a well-defined value E and that their direction of incidence was equally well defined. In fact, even when being considered as absolutely monoenergetic when leaving the accelerator tube, the electrons have to traverse a window, helium gas, and the specimen itself. The energy losses and the angular deviations of the incident electrons must then be taken into account when calculating $\sigma(E)$, where E is now the initial energy of the electron beam. Details of these corrections are given in Ref. 34.

Particularly important for the discussion of the single-crystal results is the problem of the angular dispersion of the electron beam; here, this effect is no longer a mere correction but contributes directly in the displacement mechanism. The angular distribution of the electrons can be represented by a Gaussian[36]:

$$P(\alpha) = (2/\pi\alpha)\exp(-\alpha^2/2\langle\alpha^2\rangle) \ , \qquad (7)$$

where $\langle\alpha^2\rangle = 2\theta_1^2 \ln(65.3\beta\gamma\theta_1 Z^{-1/3})$ and $\theta_1^2 = 4\pi N x Z^2 \times e^4/m_0^2 v^4\gamma^2$; Z, N, and x are the atomic number, the density of atoms per cm^3, and the thickness of the penetrated matter; e, m_0, and v are the electron charge, its rest mass, and velocity; $\beta = v/c$ and $\gamma = (1-\beta^2)^{-1/2}$. We have calculated the angular dispersion for our experimental conditions when just entering the specimen ($x = 0$), when reaching the center of it ($x = \frac{1}{2}x_0$), and after having passed through the whole of it ($x = x_0$). Table IV gives the results for specimens of $x_0 = 20$ μ and for three different electron energies. We see that irradiating a zinc specimen with electrons just above threshold (0.5 MeV) will cover practically all the crystallographic directions; we shall always observe the easiest displacement mechanism and no threshold anisotropy will be visible. In this sense, it is more favorable to work with heavier elements which have higher thresholds (like cadmium, where $E_d \approx 0.6$ MeV). We shall take this effect into account when treating our model in Paper II.

A final remark concerning the characteristic Frenkel-pair resistivity ρ_F. When comparing resistivity-change rates for different specimens, one must not forget that not only the concentration of the defects responsible for the measured effect can vary with the orientation, but also the electrical resistivity of the defect itself (expressed as ρ_F). For highly anisotropic material such as zinc and cadmium, the electrical resistivity ρ_L of the lattice is known to be a function of the crystallographic orientation of a single crystal.[37] An empirical relationship between ρ_F and ρ_L has been established by Lucasson and Walker,[38] and the results of Coltman *et al.*[22] show that the Frenkel-pair resistivities measured parallel to and perpendicular to the c axis of a cadmium crystal are roughly proportional to

TABLE IV. Angular dispersion of electrons at different levels for 20-μ-thick specimens expressed in degrees.

	zinc			cobalt			cadmium		
E/MeV	0	$\frac{1}{2}x_0$	x_0	0	$\frac{1}{2}x_0$	x_0	0	$\frac{1}{2}x_0$	x_0
0.7	9	14	18	8	14	18	10	17	24
0.5	11	18	23	10	18	24	14	24	31
0.4	14	22	28	13	22	29	17	29	38

the respective bulk resistivities at 0 °C: $\rho_F^{\parallel}/\rho_F^{\perp} \approx \rho_0^{\parallel}/\rho_0^{\perp}$. In fact, one can regard the effect of a Frenkel defect upon the scattering of a conduction electron as something like a frozen-in phonon contribution. Actually in our mounted specimens, the measuring currents for the orientations (0001) and $(11\bar{2}0)$ were always parallel to the basal plane for both zinc and cadmium, and under an angle of 60° to it for $(30\bar{3}4)$ zinc and 20° for $(30\bar{3}8)$ cadmium; thus, we do not expect any anisotropy manifestation from this direction.

V. CONCLUSIONS

We have irradiated monocrystalline specimens of cobalt, zinc, and cadmium of various orientations and have measured the corresponding resistivity change rates and annealing spectra. The following characteristic features were observed:

(i) In cobalt, the maximum defect production rate occurred for the specimen bombarded perpendicular to the (0001) plane, the minimum rates were measured for the $(11\bar{2}0)$ samples. The apparent threshold energies vary between 450 and 500 keV, in the likely order: (0001), $(30\bar{3}4)$ and $(10\bar{1}0)$, $(30\bar{3}8)$, $(11\bar{2}0)$. Orientation-dependent differences in the structure of annealing stage *I* were largest between the $(11\bar{2}0)$ and (0001) samples, at low energies.

(ii) For zinc, there are no different thresholds distinguishable because of the big angular spread of the electrons at the relatively low threshold energy of ~350 keV. The production rates increase in the order (0001), $(11\bar{2}0)$, $(30\bar{3}4)$. Maximum recovery of the entire stage *I* is observed for the (0001) sample, while the various substages behave quite differently as a function of orientation.

(iii) In cadmium, complex subthreshold behavior was observed and attributed to impurity effects. After separation of these phenomena, we deduce a minimum E_d of about 630–650 keV for the (0001) orientation; after a size-effect correction, the measured resistivity-change rates are smallest for (0001) and biggest for $(11\bar{2}0)$ crystals, with $(30\bar{3}8)$ intermediate. Two recovery regions, 4–6 °K and 6–9 °K, form the annealing stage *I*; at 0.7 MeV, the $(30\bar{3}8)$ orientation exhibits the smallest recovery in the first region; at 1.7 MeV it shows maximum recovery in both regions.

ACKNOWLEDGMENTS

The authors express their gratitude to Professor Y. Cauchois, Head of the Laboratory, whose interest in this work made it possible. It is a pleasure to acknowledge the cooperation of Professor C. Minier and her team in the initial phase of this research. Thanks are due to the accelerator team and particularly to R. Peltier for clever monitoring of the electron beam and to A. Saes who assumed helium liquefaction. Y. Loreaux's help in various technical problems is also appreciated.

[1] J. B. Gibson, A. N. Goland, M. Milgram, and G. H. Vineyard, Phys. Rev. **120**, 1229 (1960).
[2] C. Erginsoy, G. H. Vineyard, and A. Englert-Chwoles, Phys. Rev. **133**, 595 (1964).
[3] R. v. Jan and A. Seeger, Phys. Status Solidi **3**, 465 (1963).
[4] W. Kohn, Phys. Rev. **94**, 1409 (1954).
[5] W. L. Brown and W. M. Augustyniak, J. Appl. Phys. **30**, 1300 (1959).
[6] I. N. Haddad and P. C. Banbury, Philos. Mag. **14**, 829 (1966); Philos. Mag. **14**, 841 (1966).
[7] P. L. F. Hemment and P. R. C. Stevens, J. Appl. Phys. **40**, 4893 (1969).
[8] T. Iwata and T. Nihira, Phys. Lett. **23**, 631 (1966); J. Phys. Soc. Jap. **31**, 1761 (1971).
[9] K. Kamada, Y. Kazumata, and S. Suda, Phys. Status Solidi 7, 231 (1964).
[10] A. Sosin and K. Garr, Phys. Status Solidi **8**, 481 (1965).
[11] W. Bauer and A. Sosin, J. Appl. Phys. **35**, 703 (1964).
[12] W. Bauer, A. I. Anderman, and A. Sosin, Phys. Rev. **185**, 870 (1969).
[13] J. N. Lomer and M. Pepper, Philos. Mag. **16**, 1119 (1967).
[14] P. Jung and W. Schilling, Phys. Rev. B **5**, 2046 (1972).
[15] M. Biget, P. Vajda, A. Lucasson, and P. Lucasson, Radiat. Eff. (to be published).
[16] M. J. Makin, in *Atomic Collision Phenomena in Solids*, edited by D. W. Palmer, M. W. Thompson, and P. W. Townsend (North-Holland, Amsterdam, 1970), p. 205.
[17] A. Bourret, Phys. Status Solidi A **4**, 813 (1971).
[18] L. M. Howe, Philos. Mag. **22**, 965 (1970).
[19] A. Lucasson, P. Lucasson, Y. Cusson, and R. M. Walker, in International Conference on the Properties of Reactor Materials, Berkeley, England, 1961 (unpublished).
[20] A. B. Pruitt and R. L. Chaplin, Radiat. Eff. **11**, 119 (1971).
[21] R. E. Longshore and R. L. Chaplin, J. Appl. Phys. **40**, 351 (1969).
[22] R. R. Coltman, C. E. Klabunde, J. K. Redman, and A. L. Southern, Radiat. Eff. **7**, 235 (1971).
[23] F. Maury, P. Vajda, A. Lucasson, P. Lucasson, G. Roux, and C. Minier, Philos. Mag. **22**, 1265 (1970).
[24] F. Maury, G. Roux, P. Vajda, C. Minier, A. Lucasson, and P. Lucasson, Cryst. Lattice Defects **1**, 361 (1970).
[25] W. E. Faust, T. N. O'Neal, and R. L. Chaplin, Phys. Rev. **183**, 609 (1969).
[26] T. N. O'Neal and R. L. Chaplin, Phys. Rev. B **5**, 3810 (1972).
[27] F. Maury, P. Vajda, A. Lucasson, and P. Lucasson, Radiat. Eff. **10**, 239 (1971).
[28] F. Maury, A. Lucasson, and P. Lucasson, Cryst. Lattice Defects **2**, 47 (1971).
[29] M. Biget, F. Maury, P. Vajda, A. Lucasson, and P. Lucasson, Radiat. Eff. **7**, 223 (1971).
[30] C. G. Shirley and R. L. Chaplin, Phys. Rev. B **5**, 2027 (1972).
[31] W. J. McGTegart, *The Electrolytic and Chemical Polishing of Metals* (Pergamon, New York, 1959).
[32] Y. Cauchois, H. Bruck, P. Ehinger, A. Gazai, and M. Boivin, J. Phys. Radium **20**, 110A (1959).
[33] A. Lucasson, P. Lucasson, and G. Lelogeais, Cryogenics **6**, 169 (1966).
[34] F. Maury, thesis (University of Paris at Orsay, 1973) (unpublished).
[35] G. Sulpice, C. Minier, P. Moser, and H. Bilger, J. Phys. (Paris) **29**, 253 (1968).
[36] N. F. Mott and H. S. W. Massey, *The Theory of Atomic Collisions* (Clarendon, Oxford, England, 1949), p. 195.
[37] B. N. Aleksandrov and I. G. Dyakov, Zh. Eksp. Teor. Fiz. **43**, 852 (1962) [Sov. Phys.-JETP **16**, 603 (1963)].
[38] P. Lucasson and R. M. Walker, Phys. Rev. **127**, 1130 (1962).